Development of Narrow Spectrum ATP-competitive Kinase Inhibitors as Probes for BIKE and AAK1

Rafael M. Couñago[1], Alison D. Axtman[2,3], Stephen J. Capuzzi[3], Hátylas Azevedo[4], David H. Drewry[2,3], Jonathan M. Elkins[1,5], Opher Gileadi[1,5], Cristiano R. W. Guimarães[4], Alessandra Mascarello[4], Ricardo A. M. Serafim[1], Carrow I. Wells[2,3], Timothy M. Willson[2,3], William J. Zuercher[2,3,*]

[1]Structural Genomics Consortium, Universidade Estadual de Campinas — UNICAMP, Campinas, SP, Brazil.

[2]Structural Genomics Consortium, UNC Eshelman School of Pharmacy, University of North Carolina at Chapel Hill, Chapel Hill, NC, USA.

[3]Division of Chemical Biology and Medicinal Chemistry, UNC Eshelman School of Pharmacy, University of North Carolina at Chapel Hill, Chapel Hill, NC, USA.

[4]Aché Laboratórios Farmacêuticos SA, Guarulhos, SP, Brazil.

[5]Structural Genomics Consortium and Target Discovery Institute, Nuffield Department of Clinical Medicine, University of Oxford, Old Road Campus Research Building, Oxford, OX3 7DQ, UK.

*Correspondence to W. Zuercher, email: william.zuercher@unc.edu

ABSTRACT: Understanding the structural determinants of inhibitor selectivity would facilitate the design and preparation of kinase probes. We describe a pair of matched compounds differing only by one degree of saturation but showing dramatic differential activities at select kinases. We utilized x-ray crystallography and computational analysis to rationalize the basis of the differential activity.

INTRODUCTION

The human protein kinases are a family of over 500 enzymes that are involved in critical aspects of cell signaling but are often dysregulated in disease, especially cancer [1]. Protein kinases catalyze the transfer of phosphate from the cofactor ATP to their substrate proteins. Although ATP-competitive protein kinase inhibitors have been successfully developed to treat a range of cancers, inflammatory and fibrotic diseases, the function of a large number of the enzymes remains unknown [2]. Potent and selective small molecule inhibitors are powerful tools to probe the biology of these understudied kinases [3].

Because ATP-competitive inhibitors bind to a common active site, they often show activity across multiple kinases. For example, staurosporine inhibits more than 200 protein kinases. These broad spectrum inhibitors are useful for initial biochemical characterization but have little utility as probes of kinase biology [4]. By contrast, other ATP-competitive inhibitors possess activity on only a handful of kinases. These narrow spectrum inhibitors have found utility in exploring the function of several historically understudied kinases [5].

39 To strengthen the conclusions drawn from use of narrow spectrum kinase inhibitors, a
40 recently established best practice is to use the probe molecule in parallel with a
41 negative control, a closely-related analogue that is inactive for the target kinase [6].
42 Demonstration of divergent results between the probe inhibitor and its negative control
43 increases confidence that the engagement of the target kinase was responsible for the
44 observed biology.

45 For ATP-competitive kinase inhibitors, a systematic approach to develop negative
46 control analogs is to synthesize a molecule that lacks the ability to form the critical hinge
47 binding interaction, typically composed of one or more hydrogen bonds with the highly
48 conserved hinge region in the enzyme [7]. These modifications result in "kinase dead"
49 analogues. Unfortunately, kinase dead analogues often lose affinity not only for the
50 primary target kinase but also for all other off-target kinases. New strategies to create
51 kinase probe negative controls that lose affinity selectively for their target kinase are
52 needed.

53 Here we describe a pair of compounds in which a minor structural change—namely, the
54 inclusion of a cyclopropyl versus an isopropyl substituent proximal to the hinge-binding
55 moiety—leads to unexpectedly large changes in activity within a small subset of protein
56 kinases but no change against many others. We used X-ray crystallography and
57 computational models to study the molecular basis for these differential effects on
58 affinity within the target and off-target kinases in an attempt to define general
59 approaches to design selective negative control analogs.

60 **RESULTS**

61 As part of a large-scale selectivity screen of ATP-mimetic kinase inhibitors, we identified
62 a pair of very closely related 3-acylaminoindazoles (**1** and **2**) that displayed a narrow
63 binding spectrum in the KINOMEscan panel of over 400 human protein kinase assays at
64 an inhibitor concentration of 1 µM (**S1 Table**). Structurally, **1** and **2** differed only by the
65 addition of two hydrogen atoms in the change from a cyclopropyl to isopropyl
66 carboxamide. **1** and **2** had several common kinase targets but also showed some degree
67 of divergence in kinase affinity profiles. A more detailed analysis of their binding
68 characteristics revealed that **1** had submicromolar affinity for 11 kinases and weaker
69 affinity for 2 additional kinases (**Table 1**), while **2** showed submicromolar affinity for
70 7/11 of the primary kinase targets and 1/2 of the minor targets. For most of these
71 kinases, only marginal differences in potency were observed between the analogs (<3-
72 fold). However, four kinases (AAK1, BIKE, RIOK1, and RIOK3) displayed remarkable
73 differential affinity between the cyclopropyl analog **1** and isopropyl analog **2** with a
74 preference for the former (27–150-fold).

75 **Table 1**. K_d values for selected kinases. K_d values were determined for kinases observed
76 to have >70% displacement of immobilized ligand with either **1** or **2** in a KINOMEscan
77 screen at 1 µM compound.

Kinase	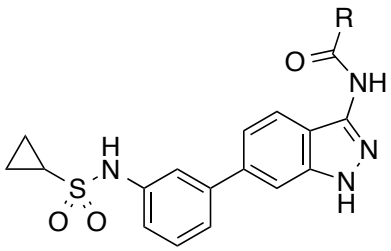	K_d **Ratio 2:1**

	1 (R = cyclopropyl) K_d (nM)	**2** (R = *i*-Pr) K_d (nM)	
AAK1	71	8800	124
BIKE	68	>10000	>150
BRAF	100	52	0.52
RIOK1	170	9600	56
PDGFRB	250	61	0.24
KIT	290	77	0.27
RIOK3	300	8200	27
DDR1	400	150	0.38
ABL1	540	190	0.35
RAF1	580	350	0.60
PDGFRA	590	240	0.41
CSF1R	2000	1600	0.80
p38a	6900	550	0.08

78

79 AAK1 and BIKE, along with the related GAK and STK16, comprise the Numb-associated
80 kinase (NAK) subfamily of protein kinases [8]. NAK family members have been proposed
81 as potential drug targets for a wide range of therapeutic areas, including virology,
82 oncology, neurology, and ophthalmology [9-12]. In contrast, relatively little is known
83 about the relevance to cellular processes of the atypical kinases RIOK1 and RIOK3.
84 Accordingly, to explore the molecular basis of the remarkable differential activities of **1**
85 and **2**, we decided to study their interaction with the NAK family kinases. **1** and **2** were
86 evaluated in FRET-based ligand binding displacement assays for all four NAK family
87 members [13]. The cyclopropyl analog **1** showed >300-fold higher affinity for AAK1 and
88 BIKE relative to the isopropyl analog **2** (**Table 2**). Both compounds demonstrated weaker
89 affinity for GAK and STK16, although a >50-fold preference for **1** relative to **2** was
90 observed with the latter kinase.

91 **Table 2**. NAK family FRET-based binding displacement assay results.

Kinase	K_i (nM)		Ratio
	1	**2**	
AAK1	8.3	2700	320
BIKE	13	3100	240
GAK	1600	4900	3
STK16	330	19000	58

92

93 *Structural analysis of compound **1** binding***.** BIKE and AAK1 are the closest members
94 within the NAK family and share a high sequence identity—74% over their kinase
95 domains and 81% within their ATP-binding sites. In order to obtain insights into the
96 molecular details of ligand interactions with these kinases, we determined the cocrystal
97 structure of BIKE kinase domain bound to compound **1** (**Table 3**), reasoning that both
98 kinases are likely to interact with **1** and **2** in similar manners.

99 **Table 3**. Crystal structure data collection and refinement statistics.

Protein	BIKE
Ligand	**1**
X-ray source	DLS I02
a (Å)	41.96
b (Å)	111.15
c (Å)	164.05
α, β, γ (^{o})	90, 90, 90
Space group	I 2 2 2
Wavelength (Å)	0.97949
Resolution limit (Å)*	28.6-2.41 (2.50-2.41)
Number of observations*	81.078 (7.855)
Completeness (%)*	99.1 (95.2)
Multiplicity*	5.3 (5.2)
Rmerge (%)*	0.074 (0.49)
Mean I/σI *	13.2 (3.1)
Refinement	
Resolution Range (Å)	21.75-2.41

Rcryst	0.176
Rfree	0.216
No. protein atoms	2,317
No. ligand atoms	28
No. solvent atoms	89
Mean B-factor (Å)	53.1
Rmsd bond lengths (Å)	0.010
Rmsd bond angles (˚)	1.04
Ramachandran statistics (%)	
Favored	98.3
Allowed	1.7
Outlier	0
PDB ID	5IKW
Crystallization conditions	10% (v/v) Broad MW PEG smear, 3.2 M $MgCl_2$, 100 mM Hepes pH 7.0

100 * Highest resolution shell shown in parentheses.

101 BIKE-**1** crystals diffracted to 2.4 Å and contained a single protein chain per asymmetric
102 unit (chain A). Sorrell and colleagues have recently reported the structural
103 characterization of all four NAK family member kinase domains, including BIKE and AAK1
104 [8]. As previously observed, our structure of BIKE displayed a catalytically-competent
105 conformation in which residues in the protein regulatory spine ("R spine"; residues M99,
106 Y111, H178 and F199) are aligned and side-chain atoms from conserved residues in β3
107 and α-C (K79 and E95, respectively) form an ion pair [14, 15]. Moreover, the NAK family-
108 exclusive helical domain (P209 to Y224) found C-terminal of the activation segment
109 (from ^{198}DFG to APE^{233} domains), dubbed ASCH (activation segment C-terminal helix) [8,
110 16, 17], also displayed an identical conformation in the BIKE structure described here
111 (**Figure 1a**).

112 **Figure 1.** Crystallographic characterization of BIKE bound to 3-acylaminoindazole **1**. (**a)**
113 BIKE-**1** adopts an active conformation. Protein (cartoon) regions important for activity
114 and ligand interaction are indicated and highlighted in different colors. As for other
115 NAK-family members, the activation segment of BIKE (orange) contains a C-terminal
116 helical segment (ASCH; in red). Inhibitor **1** (carbon atoms in pink) and BIKE residues
117 (carbon atoms in yellow) taking part in the regulatory hydrophobic spine and the critical
118 ion pair leading to an active conformation are shown as sticks. (**b**) Details of the BIKE-**1**
119 interactions. Inhibitor **1** is anchored to the hinge (green ribbon) via hydrogen bonds
120 (dashed lines) and complements the hydrophobic cavity formed by aliphatic side chains
121 from p-loop (purple ribbon) and β-6 residues. Potential interactions between main chain
122 carbonyl and the cyclopropane group are indicated by dashed lines. Hydrogen bonds
123 between Asn185, Gln137 and the sulfonamide group are also shown (dashed lines). (**c**)
124 Superposition of NAK family proteins AAK1 (blue; PDB ID 4WSQ), BIKE (grey, PDB IDs
125 5IKW, this work), GAK (PDB ID 4Y8D) and MPSK1 (PDB ID 2BUJ) shows variation in the p-
126 loop region despite good alignment in the hinge region. Compound anchoring hydrogen
127 bonds are shown for BIKE and **1** (sticks). (**d**) Electron density (2Fo-Fc) maps (grey mash;
128 1.0 σ contour) for **1**. (**e**) Primary sequence comparison of NAK family hinge and P-loop
129 regions.

130 The cocrystal structure of **1** and BIKE reveals that 3-acylaminoindazole **1** is anchored to
131 the protein hinge region (BIKE residues 131-137) *via* hydrogen bonds between the N
132 atoms of the indazole group and main chain carbonyl and NH groups of residues G131
133 and C133, respectively. An additional hydrogen bond is made between the amino group

134 of **1** and the carbonyl group of C133. At the other end of the inhibitor, the sulfonamide
135 group engages residues Q137 and N185 via hydrogen bonds. These interactions position
136 the pendant aliphatic group into a hydrophobic cavity within the P-loop formed by
137 residues V65 and S65. The indazole and the aniline rings are not coplanar to each other.
138 This flexibility provides excellent shape-complementarity between the inhibitor and the
139 ATP-binding pocket; especially with the aliphatic side chains from L187 and from p-loop
140 residues L57, A58 and V65. There is also a sulfur-π interaction between the aniline ring
141 and the sulfur atom of C197 (**Figure 1b**). Residue C197 is adjacent to the protein DFG
142 motif and has been proposed as a site of covalent modification by the inhibitor (5*Z*)-7-
143 oxozeaenol [8]. The cyclopropane group adjacent to the carboxyl group in **1** is
144 accommodated within a sharp turn of the peptide backbone involving residues
145 occupying positions +3, +4 and +5 from the so-called gatekeeper, or GK, residue (M130
146 in BIKE). This kink in the peptide backbone allows the carbonyl groups of residues GK+3
147 (C133) and GK+4 (R134) to point towards the cyclopropyl C-H group, approaching at a
148 distance of 3.6 and 3.3 Å, respectively (**Figure 1b**).

149 We compared our BIKE-**1** structure with published structures of DDR1 (PDB: 5FDP),
150 BRAF (PDB: 4XV9), AAK1 (PDB: 4WSQ), and RIOK1 (PDB: 4OTP) to attempt to rationalize
151 the structural basis differential activity of **1** and **2** on some but not all kinases. Surface
152 electrostatic potential is quite different for kinases that show differential activity
153 compared with those that do not. AAK1, BIKE, and RIOK1 have bland surface charge
154 where the critical cyclopropyl moiety of **1** is accommodated within the binding pocket.

155 In contrast, BRAF and DDR1 have highly charged surfaces around their
156 corresponding hinge binding regions.

157 Superimposing our BIKE-**1** structure with the previously published structures from the
158 NAK family [8] by aligning the hinge residues (rmsd < 0.3 Å for 7 equivalent Cα) revealed
159 that the P-loop of STK16 and GAK are substantially displaced compared to the position
160 occupied by this region in BIKE and AAK1 structures (**Figure 1d**). The extensive contacts
161 **1** makes with the P-loop may explain its selectivity for BIKE and AAK1 over the other two
162 members of the NAK family. Interestingly, the primary sequence alignment of NAK
163 family members reveals that sequence conservation is high for the P-loop region and
164 low for the hinge moiety (**Figure 1e**).

165 *Computational studies*. A range of computational methodologies was applied to shed
166 light on the differential affinities of **1** and **2**. Energy minimization calculations in the
167 unbound state using the OPLS3 force field [18] and the GB/SA [19] solvation model
168 suggest that dehydration penalty upon binding is not a dominant factor, as similar
169 hydration values were obtained for **1** (-29.8 kcal/mol) versus **2** (-29.2 kcal/mol); the
170 cyclopropyl analog was actually slightly more penalized. To investigate the electronic
171 properties, electrostatic potential derived atomic charges using the B3LYP exchange-
172 correlation energy functional [20] and the 6-31G** basis set [21] were obtained in the
173 gas phase. In this case, striking differences were observed for the C-H bond adjacent to
174 the carbonyl group; it was much more polarized for cyclopropyl than isopropyl (**Figure**
175 **2**), with no major differences for the adjacent amide.

176 **Figure 2.** Computationally generated electrostatic potential (ESP) derived atomic
177 charges for (A) **2** and (B) **1**.

178 Beyond defining potential enthalpic differences between cyclopropyl and isopropyl
179 substituents, we also investigated possible entropic differences between **1** and **2** for
180 selected kinases. The Glide docking application was used to predict binding poses in
181 each investigated kinase, and the components of entropy change (translational,
182 rotational, and vibrational) upon binding of **1** and **2** to the kinases were calculated using
183 the RRHO approximation (**Table 4**). Translational and rotational entropic losses were
184 essentially equivalent for **1** and **2** at any given kinase. However, the vibrational entropic
185 gain was higher for **1** with all kinases except p38α. Interestingly, upon binding, the
186 largest overall changes in entropy, or $\Delta(T\Delta S_{bind})$, between **1** and **2** were observed for
187 AAK**1** and BIKE. These two kinases displayed the two largest K_d ratios. $\Delta(T\Delta S_{bind})$
188 between **1** and **2** was markedly lower for those kinases not displaying significant activity
189 cliffs. However, there are two exceptions to this observation, namely KIT and RIOK1. The
190 former displayed a significant $\Delta(T\Delta S_{bind})$ between **1** and **2**, although there is not a
191 significant difference in affinity. With RIOK**1**, the entropic difference between **1** and **2**
192 was modest, despite a K_d ratio **2**:**1** of 56 (**Table 1**).

193 **Table 4.** Thermodynamic parameters of binding **1** and **2** with kinases.

Kinase	PDB	Cmpd	$T\Delta S_{bind}$				$\Delta(T\Delta S_{bind})$
			Trans	Rot	Vib	Total	
AAK1	5L4Q	**1**	-11.30	-11.14	4.70	-17.75	3.54
		2	-11.31	-11.07	1.09	-21.29	
BIKE	5IKW	**1**	-11.30	-11.07	4.64	-17.73	2.51
		2	-11.31	-11.10	2.17	-20.24	

p38a	5LAR	**1**	-11.30	-11.13	3.35	-19.09	-0.10
		2	-11.31	-11.17	3.49	-18.98	
ABL	4ZOG	**1**	-11.30	-11.05	3.15	-19.20	1.64
		2	-11.31	-11.04	1.51	-20.84	
KIT	4U0I	**1**	-11.30	-11.13	3.09	-19.34	3.23
		2	-11.31	-11.18	-0.08	-22.57	
DDR1	5FDP	**1**	-11.30	-11.06	3.84	-18.52	1.45
		2	-11.31	-11.08	2.41	-19.97	
CSF1R	4R7H	**1**	-11.30	-11.10	2.21	-20.19	1.07
		2	-11.31	-11.10	1.14	-21.27	
RIOK1	4OTP	**1**	-11.30	-11.03	6.66	-15.68	0.64
		2	-11.31	-11.10	6.09	-16.32	
RAF1	3OMV	**1**	-11.30	-11.06	2.82	-19.54	1.52
		2	-11.31	-11.09	1.34	-21.06	

DISCUSSION

The term “activity cliff” has been proposed to describe pairs of structurally similar compounds, like **1** and **2**, with a large difference in potency relative to a common target [22]. There have been other reports of kinase inhibitor activity cliffs involving cyclopropyl and isopropyl carboxamides proximal to their hinge binding moiety (**Table 5**). The 2-cyclopropylcarboxamidopyridine **3a** showed >100x higher affinity for TYK2 than the isopropyl analog **3b** [23]. This effect is not limited to binding assays as triazolopyrimidines **4** show >100x difference IC_{50} value in a JAK1 biochemical activity assay [24]. Similarly, **5a** displayed a much higher inhibition potency than **5b** in an enzymatic activity assay of mutant B-Raf^{V600E} activity [25]. These examples substantiate our observations that subtle changes in structure can lead to selective inhibition of specific protein kinases. To the best of our knowledge, **3**-**5** were not subjected to broad

207 kinome activity characterization, and the breadth of the associated activity cliffs has not

208 been evaluated.

209 **Table 5.** Previously reported matched pairs of kinase inhibitors demonstrating an affinity

210 or activity cliff between cyclopropyl and isopropyl compounds.

211

Structure	Activity
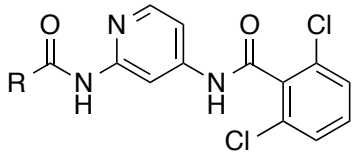 **3**	TYK2 K_i **3a** R = Cyclopropyl: 4.8 nM **3b** = Isopropyl: 840 nM Ref: [23]
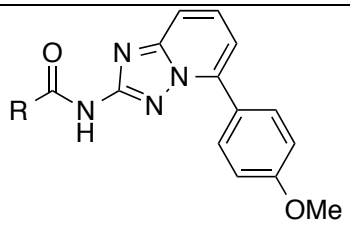 **4**	JAK1 IC_{50} **4a**: R = Cyclopropyl: 60 nM **4b**: R = Isopropyl: >10000 nM Ref: [24]
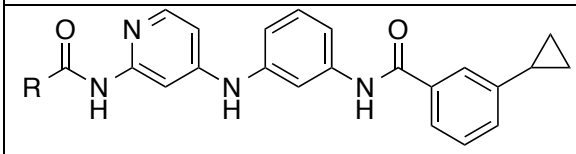 **5**	B-Raf^{V600E} IC_{50} **5a**: R = Cyclopropyl: 35 nM **5b**: R = Isopropyl: 420 nM Ref: [25]

212

213 The cyclopropyl ring is a versatile lipophilic group that frequently appears in preclinical

214 and clinical candidate molecules. It has been described to have “magical” properties

215 that can enhance potency, reduce off-target effects, increase metabolic stability and

216 brain permeability, yet the precise molecular basis for these effects remains poorly

217 understood [26]. Theoretical studies on cyclopropane and its derivatives suggest that

218 atomic bonding results mainly from the overlap of three sp^2 hybrids (one on each

219 carbon) pointing towards the center of the ring. Thus, the electron distribution in the C-

220 C internuclear region is not concentrated along the line between the nuclei, but rather
221 slightly outside this line. As a consequence, the C-C bonds have enhanced π character,
222 and the C-H bonds have more *s* character. In other words, the cyclopropyl ring behaves
223 much like an alkene, interacts with neighboring π-electron systems, and has CH bonds
224 with increased acidity relative to standard alkanes [27]. These effects are apparent
225 when the emerging negative charge on the C-H carbon is stabilized by conjugation, such
226 as the one between the π-like cyclopropyl and an amide carbonyl group in **1**. Calculated
227 electrostatic potential charges, as demonstrated above, may contribute to the activity
228 difference between **1** and **2**.

229 3-Acylaminoindazoles are a known class of ATP-competitive protein kinase inhibitors
230 [28]. The heterocyclic core mimics the adenosine base of ATP and forms hydrogen
231 bonds with the hinge motif of the enzyme. **1** and **2**, differing by only two hydrogen
232 atoms were screened across 400 human protein kinases to define both compounds as
233 narrow spectrum inhibitors, with high affinity binding to <3% of the kinases surveyed.
234 Both **1** and **2** bound to seven kinases (ABL1, BRAF, DDR1, KIT, PDGFRA, PDGFRB, and
235 RAF1) with submicromolar affinity. Surprisingly, cyclopropyl amide **1** bound to an
236 additional four kinases (AAK1, BIKE, RIOK1, and RIOK3) where isopropyl amide **2** was not
237 effective. Thus, this pair of ATP-competitive kinase inhibitors have the potential to be
238 used to probe selectively the biology of just 4 protein kinases while controlling for over
239 400 others in the human genome.

240 BIKE and AAK1 are both members of the NAK (Numb-associated kinase) family of
241 protein kinases and share close sequence identity within their catalytic sites. Both
242 kinases are potently inhibited by the 3-acylaminoindazole **1** and are likely to interact
243 with the inhibitor through conserved interactions. The BIKE-**1** cocrystal structure
244 provides a clear view into the molecular details of the enzyme-ligand interaction. The
245 critical cyclopropyl carboxamide sits in a pocket adjacent to the hinge-binding residues
246 and is orientated toward the protein surface. The amide NH of **1** and the cyclopropyl
247 ring C-H sit in close proximity (2.70 and 3.29 Å, respectively) to the Cys133 carbonyl
248 oxygen (**Figure 3**). Our quantum mechanical calculations showed that the cyclopropyl
249 group has an increased polarization across the ring C-H compared the corresponding
250 isopropyl analogue. The complex between the cyclopropyl derivative **1** and BIKE is
251 indicative of a CH-O nonconventional hydrogen bond. Electrostatic interactions
252 dominate hydrogen bonds and the increased polarization of the cyclopropyl C-H bond,
253 as evidenced by the electrostatic potential charges, may explain why **1** shows
254 significantly higher affinity for AAK1 and BIKE than the isopropyl analog **2** but leaves
255 unanswered the question about why **1** and **2** are equipotent at other kinases.

256 **Figure 3.** (A) **1** bound in BIKE active site. (B) Two dimensional compound interaction
257 diagram of **1** and BIKE depicting adjacent residues and key interactions.

258 Modulating entropy contributions has previously been proposed as a means to increase
259 binding affinity between small molecules and proteins [29]. Upon binding, ligands lose
260 degrees of freedom with respect to translational, rotational, and vibrational motion.

261 This loss of freedom constitutes a loss of entropy, which disfavors binding. Given its
262 triangular nature and smaller size, the cyclopropyl group may vibrate more freely within
263 the protein, which favor binding when compared to the isopropyl group. Importantly,
264 depending on the protein environment and architecture, this effect can be more
265 pronounced. In our cocrystal structure of BIKE and **1**, the cyclopropyl group of interest is
266 more solvent exposed. As such, this group is not as restricted by the binding site and
267 does not experience a significant loss in vibrational entropy, which may be driving the
268 activity cliff observed between **1** and **2**. Kinases for which an activity cliff between **1** and
269 **2** is not observed may have the cyclopropyl group less solvent exposed, leading to a
270 larger vibrational entropy loss.

271 We have suggested that differences in electrostatic potential or in vibrational entropy
272 changes may help to rationalize the activity cliffs between **1** and **2** in some kinases but
273 not in others. We recognize that there are myriad other subtle changes in the binding
274 pockets that must also be explored to enable prediction of which kinases can be
275 differentially inhibited by matched ligand pairs like **1** and **2**. Our enhanced
276 understanding of the differential interactions of **1** and **2** within the binding pockets of
277 AAK1, BIKE, and other kinases will improve our ability to produce narrow spectrum
278 probes with optimal negative control analogs for use in biological studies.

279 **Supporting Information**

280 **S1 Table. Results of KINOMEscan and select K_d determinations for 1 and 2.**
281 KINOMEscan assay panel and associated K_d determinations were conducted at

282 DiscoverX Corporation. Compounds were evaluated as single measurements at 1 μM.
283 Displacement percentage ("Disp %") reflects the extent to which the compound
284 displaced the kinase construct from an immobilized ligand. K_d values were determined
285 for all kinases with ≥70% displacement with **1** in the KINOMEscan screen at 1 μM
286 compound and selected other kinases.

287 **MATERIALS AND METHODS**

288 *N*-(6-(3-(cyclopropanesulfonamido)phenyl)-1*H*-indazol-3-yl)cyclopropanecarboxamide
289 (**1**). ^{1}H NMR (400 MHz, Methanol-d_4) δ 7.83 – 7.78 (d, *J* = 8.6 Hz, 1H), 7.61 – 7.54 (m,
290 2H), 7.46 – 7.30 (m, 3H), 7.29 – 7.23 (ddd, *J* = 7.7, 2.2, 1.3 Hz, 1H), 2.62 – 2.49 (tt, *J* = 8.0,
291 4.8 Hz, 1H), 1.95 – 1.84 (ddd, *J* = 12.5, 7.9, 4.2 Hz, 1H), 1.07 – 0.77 (m, 8H). MS+ (– ES
292 API) - 397.1

293 *N*-(6-(3-(cyclopropanesulfonamido)phenyl)-1*H*-indazol-3-yl)isobutyramide (**2**). ^{1}H NMR
294 (400 MHz, Methanol-d_4) δ 7.82 – 7.75 (d, *J* = 8.6 Hz, 1H), 7.62 – 7.54 (dt, *J* = 10.9, 1.5 Hz,
295 2H), 7.47 – 7.31 (m, 3H), 7.31 – 7.22 (ddd, *J* = 7.8, 2.2, 1.3 Hz, 1H), 2.84 – 2.69 (hept, *J* =
296 6.8 Hz, 1H), 2.61 – 2.50 (tt, *J* = 8.0, 4.8 Hz, 1H), 1.29 – 1.15 (d, *J* = 6.8 Hz, 6H), 1.14 – 0.82
297 (m, 4H). MS+ (– ES API) - 399.1

298 **DiscoverX kinase affinity measurements.** KINOMEscan assay panel profiling and
299 associated K_d determinations were obtained at DiscoverX Corporation using their
300 previously described methodology [30, 31].

301 **Binding displacement assays.** Inhibitor binding was determined using a binding-
302 displacement assay, which tests the ability of the inhibitors to displace a fluorescent
303 tracer compound from the ATP binding site of the kinase domain. Inhibitors were
304 dissolved in DMSO and dispensed as 16-point, 2x serial dilutions in duplicate into black
305 multiwell plates (Greiner). Each well contained either 0.5 nM or 1 nM biotinylated
306 kinase domain protein ligated to streptavidin-Tb-cryptate (Cisbio), 12.5 nM or 25 nM
307 Kinase Tracer 236 (ThermoFisher Scientific), 10 mM Hepes pH 7.5, 150 mM NaCl, 2 mM
308 DTT, 0.01% BSA, 0.01% Tween-20. Final assay volume for each data point was 5 µL, and
309 final DMSO concentration was 1%. The plate was incubated at room temperature for 1.5
310 hours and then read using a TR-FRET protocol on a PheraStarFS plate reader (BMG
311 Labtech). The data was normalized to 0% and 100% inhibition control values and fitted
312 to a four parameter dose-response binding curve in GraphPad Software. The
313 determined IC_{50} values were converted to K_i values using the Cheng-Prusoff equation
314 and the concentration and K_d values for the tracer (previously determined).

315 **Cloning, Expression, Purification and crystallization**. $BIKE_{38\text{-}345\ (K320A,\ K321A)}$ with a tobacco
316 etch virus (TEV) protease cleavable, N-terminal 6xHis tag was expressed from vector
317 pNIC-ZB. To improve BIKE crystallization, a cluster of surface entropy reduction
318 mutations [32] was engineered into the expression construct, K320A/K321A [8]. For
319 protein production, the host *E. coli* strain, BL21(DE3)-R3 expressing lambda
320 phosphatase, was cultivated in TB medium (+ 50 µg/ml kanamycin, 35 µg/ml
321 chloramphenicol) at 37°C until OD_{600} reached ~3 and then cooled to 18°C for 1 hour.
322 Isopropyl 1-thio-D-galactopyranoside was added to 0.1 mM, and growth continued at

323 18°C overnight. The cells were collected by centrifugation then resuspended in 2x lysis
324 buffer (100 mM HEPES buffer, pH 7.5, 1.0 M NaCl, 20 mM imidazole, 1.0 mM tris(2-
325 carboxyethyl)phosphine, 2x Protease Inhibitors Cocktail Set VII (Calbiochem, 1/1000
326 dilution) and flash-frozen in liquid nitrogen. Cells were lysed by sonication on ice. The
327 resulting proteins were purified using Ni-Sepharose resin (GE Healthcare) and eluted
328 stepwise in binding buffer with 300 mM imidazole. Removal of the hexahistidine tag was
329 performed at 4°C overnight using recombinant TEV protease. Proteins were further
330 purified using reverse affinity chromatography on Ni-Sepharose followed by gel
331 filtration (Superdex 200 16/60, GE Healthcare). Protein in gel filtration buffer (25 mM
332 HEPES, 500 mM NaCl, 0.5 mM TCEP, 5% [v/v] glycerol) was concentrated to 12 mg/ml
333 using 30 kDa MWCO centrifugal concentrators (Millipore) at 4°C. 3-acylaminoindazole **1**
334 in 100% DMSO was added to the protein in a 3-fold molar excess and incubated on ice
335 for approximately 30 minutes. The mixture was centrifuged at 14,000 rpm for 10
336 minutes at 4°C prior to setting up 150 nL volume sitting drops at three ratios (2:1, 1:1, or
337 1:2 protein-inhibitor complex to reservoir solution). Crystallization experiments were
338 performed at 20°C. Crystals were cryoprotected in mother liquor supplemented with 20-
339 25% glycerol before flash-freezing in liquid nitrogen for data collection. Diffraction data
340 were collected at the Diamond Light Source. The best diffracting crystals grew under the
341 conditions described in **Table 1**. When noted, crystal optimization used Newman's
342 buffer system [33] and defined PEG smears [34].

343 **Structure Solution and Refinement.** Diffraction data were integrated using XDS [35] and
344 scaled using AIMLESS from the CCP4 software suite [36]. Molecular replacement for was

345 performed with Phaser [37] using BIKE/AZD7762 (PDB ID: 4W9W) [8] as a search model.
346 Automated model building was performed with Buccanner [38]. Automated refinement
347 was performed in PHENIX [39]. Coot [40] was used for manual model building and
348 refinement. Structure validation was performed using MolProbity [41]. Structure factors
349 and coordinates have been deposited in the PDB (see Table 1).

350 **Computation**. Solvation free energies and quantum mechanical calculations were run
351 using Macromodel ([42]) and Jaguar ([43]) from Schrodinger Inc. Further computational
352 studies were performed using Maestro 11 from Schrodinger (Schrödinger Release 2016-
353 4: Maestro, Schrödinger, LLC, New York, NY, 2016). The lowest energy configurations for
354 compounds **1** and **2** at pH 7 were generated with the Ligand Preparation application
355 (Schrödinger Release 2016-4: LigPrep, Schrödinger, LLC, New York, NY, 2016). Next, PDB
356 crystal structures for AAK1, BIKE and the other kinases in Table 4 were downloaded and
357 prepared for docking. Briefly, bond orders were assigned, hydrogen atoms were added,
358 selenomethionine residues were converted to methionines, and missing side chains
359 were filled with the Prime application. The protein grid for docking was set by selecting
360 the center of the cocrystal ligand in the PDB structure. The Glide application was used
361 for docking of 1 and 2 to all kinases (Schrödinger Release 2016-4: Glide, Schrödinger,
362 LLC, New York, NY, 2016.). Flexible ligand sampling was allowed with the XP (extra
363 precision) scoring function (http://pubs.acs.org/doi/abs/10.1021/jm051256o). Once the
364 ligands were docked and the lowest energy poses were retrieved, a Rigid Rotor
365 Harmonic Oscillation (RRHO) approximation was performed on the theoretical protein-
366 ligand complex (https://www.ncbi.nlm.nih.gov/pmc/articles/PMC3329805/). For the

367 RRHO approximation, an OPLS_2005 force field was applied
368 (http://pubs.acs.org/doi/abs/10.1021/acs.jctc.5b00864).

369 **ACKNOWLEDGMENT**

370 Aled Edwards is acknowledged for illuminating discussions and encouragement in the
371 preparation of this manuscript. We thank Diamond Light Source for access to beamline
372 I03 (proposal number MX14664) that contributed to the results presented here. The
373 SGC is a registered charity (number 1097737) that receives funds from AbbVie, Bayer
374 Pharma AG, Boehringer Ingelheim, Canada Foundation for Innovation, Eshelman
375 Institute for Innovation, Genome Canada, Innovative Medicines Initiative (EU/EFPIA),
376 Janssen, Merck & Co., Novartis Pharma AG, Ontario Ministry of Economic Development
377 and Innovation, Pfizer, São Paulo Research Foundation-FAPESP, Takeda, and Wellcome
378 Trust.

379

380 **Figure 1.**

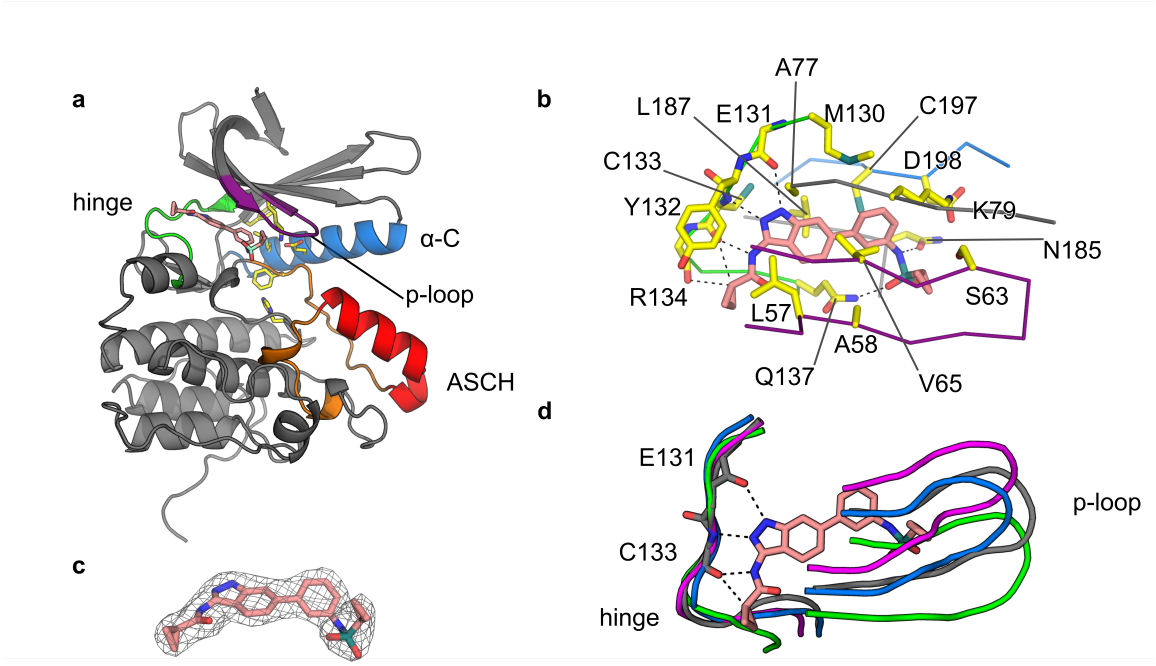

381

382

383

384 **Figure 2.**

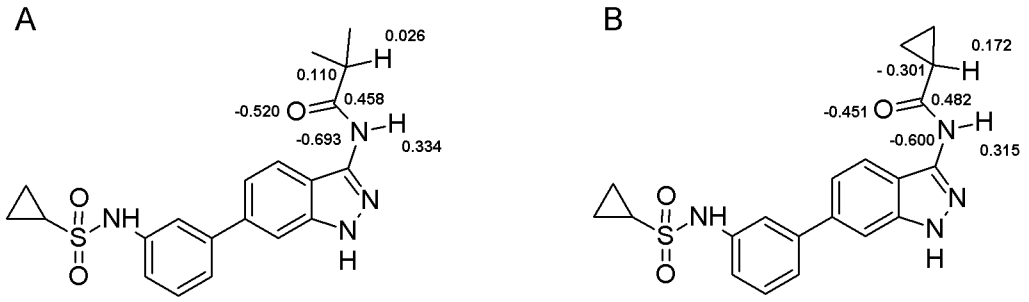

385

386

387 **Figure 3.**

A

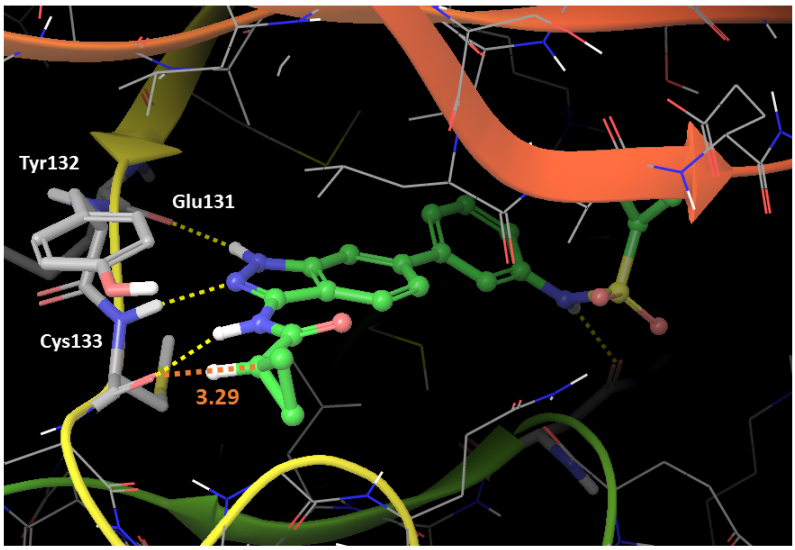

B

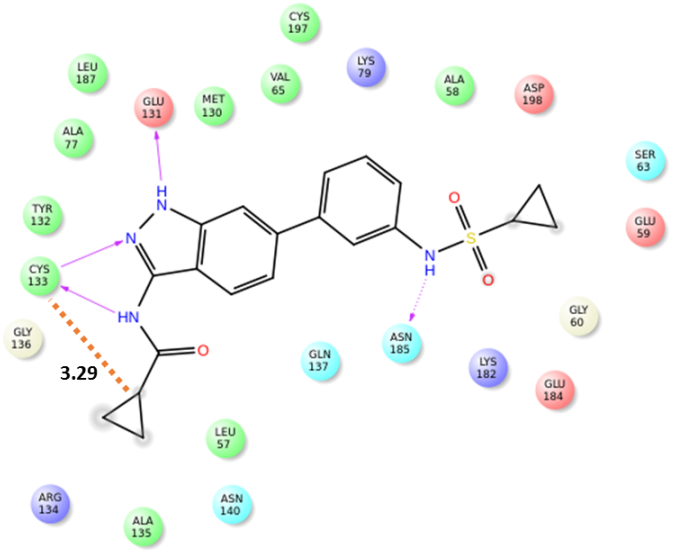

388

389 **REFERENCES**

390 1. Cohen P, Alessi DR. Kinase drug discovery--what's next in the field? ACS Chem
391 Biol. 2013;8(1):96-104. doi: 10.1021/cb300610s. PubMed PMID: 23276252; PubMed
392 Central PMCID: PMCPMC4208300.
393 2. Fedorov O, Muller S, Knapp S. The (un)targeted cancer kinome. Nat Chem Biol.
394 2010;6(3):166-9. doi: 10.1038/nchembio.297. PubMed PMID: 20154661.
395 3. Uitdehaag JC, Verkaar F, Alwan H, de Man J, Buijsman RC, Zaman GJ. A guide to
396 picking the most selective kinase inhibitor tool compounds for pharmacological
397 validation of drug targets. Br J Pharmacol. 2012;166(3):858-76. doi: 10.1111/j.1476-
398 5381.2012.01859.x. PubMed PMID: 22250956; PubMed Central PMCID:
399 PMCPMC3417414.
400 4. Ruegg UT, Burgess GM. Staurosporine, K-252 and UCN-01: potent but
401 nonspecific inhibitors of protein kinases. Trends Pharmacol Sci. 1989;10(6):218-20.
402 PubMed PMID: 2672462.
403 5. Knapp S, Arruda P, Blagg J, Burley S, Drewry DH, Edwards A, et al. A public-
404 private partnership to unlock the untargeted kinome. Nat Chem Biol. 2013;9(1):3-6. doi:
405 10.1038/nchembio.1113. PubMed PMID: 23238671.
406 6. Arrowsmith CH, Audia JE, Austin C, Baell J, Bennett J, Blagg J, et al. The promise
407 and peril of chemical probes. Nat Chem Biol. 2015;11(8):536-41. doi:
408 10.1038/nchembio.1867. PubMed PMID: 26196764.
409 7. Xing L, Klug-Mcleod J, Rai B, Lunney EA. Kinase hinge binding scaffolds and their
410 hydrogen bond patterns. Bioorg Med Chem. 2015;23(19):6520-7. doi:
411 10.1016/j.bmc.2015.08.006. PubMed PMID: 26358279.
412 8. Sorrell FJ, Szklarz M, Abdul Azeez KR, Elkins JM, Knapp S. Family-wide Structural
413 Analysis of Human Numb-Associated Protein Kinases. Structure. 2016;24(3):401-11. doi:
414 10.1016/j.str.2015.12.015. PubMed PMID: 26853940; PubMed Central PMCID:
415 PMCPMC4780864.
416 9. Liu HP, Lin YJ, Lin WY, Wan L, Sheu JJ, Lin HJ, et al. A novel genetic variant of
417 BMP2K contributes to high myopia. J Clin Lab Anal. 2009;23(6):362-7. doi:
418 10.1002/jcla.20344. PubMed PMID: 19927351.
419 10. Neveu G, Ziv-Av A, Barouch-Bentov R, Berkerman E, Mulholland J, Einav S. AP-2-
420 associated protein kinase 1 and cyclin G-associated kinase regulate hepatitis C virus
421 entry and are potential drug targets. J Virol. 2015;89(8):4387-404. doi:
422 10.1128/JVI.02705-14. PubMed PMID: 25653444; PubMed Central PMCID:
423 PMC4442395.
424 11. Sakurai MA, Ozaki Y, Okuzaki D, Naito Y, Sasakura T, Okamoto A, et al. Gefitinib
425 and luteolin cause growth arrest of human prostate cancer PC-3 cells via inhibition of
426 cyclin G-associated kinase and induction of miR-630. PLoS One. 2014;9(6):e100124. doi:
427 10.1371/journal.pone.0100124. PubMed PMID: 24971999; PubMed Central PMCID:
428 PMCPMC4074034.
429 12. Shi B, Conner SD, Liu J. Dysfunction of endocytic kinase AAK1 in ALS. Int J Mol Sci.
430 2014;15(12):22918-32. doi: 10.3390/ijms151222918. PubMed PMID: 25514244;
431 PubMed Central PMCID: PMCPMC4284746.

13. Lebakken CS, Riddle SM, Singh U, Frazee WJ, Eliason HC, Gao Y, et al. Development and applications of a broad-coverage, TR-FRET-based kinase binding assay platform. J Biomol Screen. 2009;14(8):924-35. doi: 10.1177/1087057109339207. PubMed PMID: 19564447.
14. Huse M, Kuriyan J. The conformational plasticity of protein kinases. Cell. 2002;109(3):275-82. PubMed PMID: 12015977.
15. Kornev AP, Taylor SS. Defining the conserved internal architecture of a protein kinase. Biochim Biophys Acta. 2010;1804(3):440-4. doi: 10.1016/j.bbapap.2009.10.017. PubMed PMID: 19879387; PubMed Central PMCID: PMCPMC3435107.
16. Chaikuad A, Keates T, Vincke C, Kaufholz M, Zenn M, Zimmermann B, et al. Structure of cyclin G-associated kinase (GAK) trapped in different conformations using nanobodies. Biochem J. 2014;459(1):59-69. doi: 10.1042/BJ20131399. PubMed PMID: 24438162; PubMed Central PMCID: PMCPMC3957475.
17. Eswaran J, Bernad A, Ligos JM, Guinea B, Debreczeni JE, Sobott F, et al. Structure of the human protein kinase MPSK1 reveals an atypical activation loop architecture. Structure. 2008;16(1):115-24. doi: 10.1016/j.str.2007.10.026. PubMed PMID: 18184589; PubMed Central PMCID: PMCPMC2194165.
18. Harder E, Damm W, Maple J, Wu C, Reboul M, Xiang JY, et al. OPLS3: A Force Field Providing Broad Coverage of Drug-like Small Molecules and Proteins. J Chem Theory Comput. 2016;12(1):281-96. doi: 10.1021/acs.jctc.5b00864. PubMed PMID: 26584231.
19. Still WC, Tempczyk A, Hawley RC, Hendrickson T. Semianalytical Treatment of Solvation for Molecular Mechanics and Dynamics. J Am Chem Soc. 1990;112:6127-9.
20. Stephens PJ, Devlin FJ, Chabalowski CF, Frisch MJ. J Phys Chem. 1994;98:11623.
21. Frisch MJ, Pople JA, Binkley JS. J Chem Phys. 1984:3265.
22. Stumpfe D, Bajorath J. Exploring activity cliffs in medicinal chemistry. J Med Chem. 2012;55(7):2932-42. doi: 10.1021/jm201706b. PubMed PMID: 22236250.
23. Liang J, Tsui V, Van Abbema A, Bao L, Barrett K, Beresini M, et al. Lead identification of novel and selective TYK2 inhibitors. Eur J Med Chem. 2013;67:175-87. doi: 10.1016/j.ejmech.2013.03.070. PubMed PMID: 23867602.
24. Menet CJ, Fletcher SR, Van Lommen G, Geney R, Blanc J, Smits K, et al. Triazolopyridines as selective JAK1 inhibitors: from hit identification to GLPG0634. J Med Chem. 2014;57(22):9323-42. doi: 10.1021/jm501262q. PubMed PMID: 25369270.
25. Li X, Shen J, Tan L, Zhang Z, Gao D, Luo J, et al. Design and synthesis of N-(4-aminopyridin-2-yl)amides as B-Raf(V600E) inhibitors. Bioorg Med Chem Lett. 2016;26(12):2760-3. doi: 10.1016/j.bmcl.2016.04.076. PubMed PMID: 27155899.
26. Talele TT. The "Cyclopropyl Fragment" is a Versatile Player that Frequently Appears in Preclinical/Clinical Drug Molecules. J Med Chem. 2016;59(19):8712-56. doi: 10.1021/acs.jmedchem.6b00472. PubMed PMID: 27299736.
27. Galano A, Alvarez-Idaboy J, Vivier-Bunge A. Non-alkane behavior of cyclopropane and its derivatives: characterization of unconventional hydrogen bond interactions. Theor Chem Account. 2007;118:597-606.
28. Witherington J, Bordas V, Gaiba A, Naylor A, Rawlings AD, Slingsby BP, et al. 6-heteroaryl-pyrazolo[3,4-b]pyridines: potent and selective inhibitors of glycogen

476 synthase kinase-3 (GSK-3). Bioorg Med Chem Lett. 2003;13(18):3059-62. PubMed PMID:
477 12941333.
478 29. Chang CE, Chen W, Gilson MK. Ligand configurational entropy and protein
479 binding. Proc Natl Acad Sci U S A. 2007;104(5):1534-9. doi: 10.1073/pnas.0610494104.
480 PubMed PMID: 17242351; PubMed Central PMCID: PMCPMC1780070.
481 30. Davis MI, Hunt JP, Herrgard S, Ciceri P, Wodicka LM, Pallares G, et al.
482 Comprehensive analysis of kinase inhibitor selectivity. Nat Biotechnol.
483 2011;29(11):1046-51. doi: 10.1038/nbt.1990. PubMed PMID: 22037378.
484 31. Fabian MA, Biggs WH, 3rd, Treiber DK, Atteridge CE, Azimioara MD, Benedetti
485 MG, et al. A small molecule-kinase interaction map for clinical kinase inhibitors. Nat
486 Biotechnol. 2005;23(3):329-36. doi: 10.1038/nbt1068. PubMed PMID: 15711537.
487 32. Derewenda ZS. Rational protein crystallization by mutational surface
488 engineering. Structure. 2004;12(4):529-35. doi: 10.1016/j.str.2004.03.008. PubMed
489 PMID: 15062076.
490 33. Newman J. Novel buffer systems for macromolecular crystallization. Acta
491 crystallographica Section D, Biological crystallography. 2004;60(Pt 3):610-2. doi:
492 10.1107/S0907444903029640. PubMed PMID: 14993709.
493 34. Chaikuad A, Knapp S, von Delft F. Defined PEG smears as an alternative approach
494 to enhance the search for crystallization conditions and crystal-quality improvement in
495 reduced screens. Acta crystallographica Section D, Biological crystallography. 2015;71(Pt
496 8):1627-39. doi: 10.1107/S1399004715007968. PubMed PMID: 26249344; PubMed
497 Central PMCID: PMC4528798.
498 35. Kabsch W. Xds. Acta crystallographica Section D, Biological crystallography.
499 2010;66(Pt 2):125-32. doi: 10.1107/S0907444909047337. PubMed PMID: 20124692;
500 PubMed Central PMCID: PMC2815665.
501 36. Winn MD, Ballard CC, Cowtan KD, Dodson EJ, Emsley P, Evans PR, et al. Overview
502 of the CCP4 suite and current developments. Acta crystallographica Section D, Biological
503 crystallography. 2011;67(Pt 4):235-42. doi: 10.1107/S0907444910045749. PubMed
504 PMID: 21460441; PubMed Central PMCID: PMC3069738.
505 37. McCoy AJ, Grosse-Kunstleve RW, Adams PD, Winn MD, Storoni LC, Read RJ.
506 Phaser crystallographic software. Journal of applied crystallography. 2007;40(Pt 4):658-
507 74. doi: 10.1107/S0021889807021206. PubMed PMID: 19461840; PubMed Central
508 PMCID: PMC2483472.
509 38. Cowtan K. The Buccaneer software for automated model building. 1. Tracing
510 protein chains. Acta crystallographica Section D, Biological crystallography. 2006;62(Pt
511 9):1002-11. doi: 10.1107/S0907444906022116. PubMed PMID: 16929101.
512 39. Zhang KY, Cowtan K, Main P. Combining constraints for electron-density
513 modification. Methods in enzymology. 1997;277:53-64. PubMed PMID: 18488305.
514 40. Emsley P, Lohkamp B, Scott WG, Cowtan K. Features and development of Coot.
515 Acta crystallographica Section D, Biological crystallography. 2010;66(Pt 4):486-501. doi:
516 10.1107/S0907444910007493. PubMed PMID: 20383002; PubMed Central PMCID:
517 PMC2852313.
518 41. Chen VB, Arendall WB, 3rd, Headd JJ, Keedy DA, Immormino RM, Kapral GJ, et al.
519 MolProbity: all-atom structure validation for macromolecular crystallography. Acta

520 crystallographica Section D, Biological crystallography. 2010;66(Pt 1):12-21. doi:
521 10.1107/S0907444909042073. PubMed PMID: 20057044; PubMed Central PMCID:
522 PMC2803126.
523 42. Schrödinger Release 2016-3: MacroModel, Schrödinger, LLC New York, NY, 2016.
524 43. Schrödinger Release 2016-4: Jaguar, Schrödinger, LLC, New York, NY, 2016.
525

526